AKADÉMIAI KIADÓ

UNIVERSITY of DEBRECEN

International Review of Applied Sciences and Engineering

14 (2023) 3, 366–373

DOI:
10.1556/1848.2022.00577

ORIGINAL RESEARCH PAPER

Effects of Neumann and Robin boundaries on the thermal instability

Hajar Lagziri*, Hanae El Fakiri and Abdelmajid El Bouardi

Department of Physics, Faculty of Science, University of Abdelmalek Essaadi, Tetouan, Morocco

Received: August 4, 2022 • Accepted: December 18, 2022
Published online: March 21, 2023

ABSTRACT

The thermo convective instability of the Darcy-Benard problem (DB) using Robin (third-kind) thermal conditions is investigated here. We consider a viscous Newtonian fluid saturating a porous layer in which the layer is sandwiched between two impermeable boundaries. The upper and the lower walls are modelled in the form of the Neumann (second-kind) and the Robin (third-kind) thermal conditions, respectively. The difference in the temperature distribution between both phases allows the lack of a local thermal equilibrium model to be present. As a consequence, the third kind of thermal condition brings about one extra dimensionless parameter of the Biot number to the usual one of the inter-heat transfer coefficient and the thermal conductivity ratio. The normal modes method adopted in a linear stability analysis gives rise to perturbed governing equations. The eigenvalue problem is handled numerically as a result of the perturbed governing equations leading to the marginal stability condition.

KEYWORDS

porous medium, biot number, heat flux, local thermal non-equilibrium, linear stability

1. INTRODUCTION

The Darcy-Benard problem (DB) [1], which embodies the thermo convective instability in porous media, becomes the cornerstone of many industrial and environmental applications. For instance, the onset of the convection cell accelerates the dissolution and the mixing of CO_2 in the aqueous phase, which, in turn, increases its storage lifespan in deep geological layers [2]. The emergence of this phenomenon does not only favor the process of CO_2 sequestration but also the extraction of the thermal energy from the geothermal reservoirs where the underground heating condition occurs. The main process behind the thermal instability in these fields is the prevailing effect of buoyant forces in comparison with resistive mechanisms that can be generated by viscous dissipation, thermal conductivity or other physical properties [3]. Whatever the medium in which instability arises, the motion of the fluid particles caused by buoyancy effects is always driven either by the concentration of solute particles or by the vertical temperature gradient [4, 5]. However, the materials manufactured by porous media are more effective to hasten the heat transfer process than the case of Newtonian clear fluid. The Rayleigh number R_c appears in the former configuration at the critical value of $R_c \approx 39$ while in the latter one at $R_c \approx 1707$ [6, 7].

The prevailing effects of the local thermal non-equilibrium (LTNE) render the thermal boundary conditions to be mismatched with the standard forms defined in the equilibrium one. As the temperature profile for the solid structure diverges from the fluid phase, several thermal boundaries are required to investigate the Darcy-Benard problem [8, 9]. On the other hand, whatever the type of these boundaries in a LTNE the marginal stability curves may tend to behave the same way as the standard one if the two dimensionless numbers defined by the internal heat transfer coefficient H and the thermal conductivity ratio γ resulted in the discrepancy between thermal conductivities of phases and the loss or gain of heat from one phase to another have specific values or limits. For instance, there are two possible conditions at which the transition from LTNE to LTE is acceptable: an infinite limit of H with a nonzero

*Corresponding author.
E-mail: lagziri-hajar7@hotmail.fr

AKJournals

value of γ or finite and non-vanishing values of H with large γ. The former case assures a rapid and higher amount of heat transferred between phases while the latter corresponds to a case in which the saturated fluid holds higher thermal conductance than the solid skeleton. A small H or γ can reverse the approach of the LTE towards a non-equilibrium one [10–13].

The majority of the analysis carried out in the Darcy-Benard problem is focused on the case where the local thermal equilibrium condition (LTE) takes place. In other words, the convection cell in a horizontal saturated porous layer is handled only when a Newtonian saturating fluid has a temperature field equal to a solid matrix. All these instability analyses are studied either with impermeable or permeable bounding planes beside different positions of the porous layer [14–16]. However, the feature of the LTE is not always true as we can encounter in some cases a disparity in the thermal conductivity or/and a weakness in the heat transfer coefficient, which can yield a relaxation of the local thermal equilibrium regime. From a practical standpoint, the local thermal non-equilibrium (LTNE) model has a vital effect on the cooling process of countless engineering devices [10, 17]. On the other hand, the approach of the LTNE can highlight difficulties in the modelling of thermal boundaries, especially in the case of isoflux [18–20]. The objective behind this work is to analyze the convective instability in the case where two impermeable walls are supposed to be modelled in the form of Newton's cooling law equation for Robin (third-kind) thermal conditions and uniform heat flux (Model A) for Neumann (second-kind) thermal conditions.

2. MATHEMATICAL MODEL

The setup assumed here is the archetype of the Darcy-Benard configuration (DB) with two rigid walls [1]. In addition, two different temperature fields are allowed, which enables violation of local thermal equilibrium. The upper wall is heated by a heater to yield uniform heat flux (Model A) while the lower one is determined as Newton's cooling law equation. For definiteness, our investigation has been performed with porosity $\varphi = 1/2$. A sketch of the system geometry is drawn in Fig. 1. Besides, we presume that Darcy's law and the Oberbeck-Boussinesq approximation

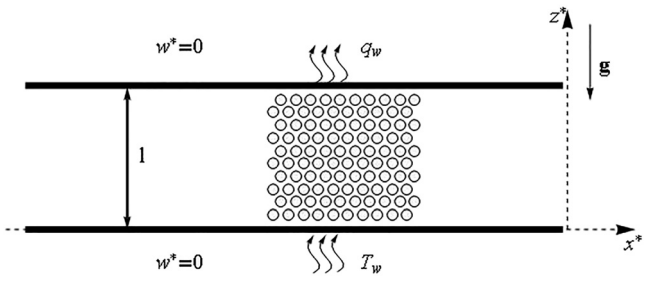

Fig. 1. The sketch of the Darcy-Benard configuration (DB)

are applicable. The governing equations in the dimensionless forms are written as [19, 12]:

$$\nabla\times\boldsymbol{v} = -\mathrm{Ra}\nabla\times\left(T_f\ \boldsymbol{e_z}\right), \tag{1a}$$

$$\chi\frac{\partial T_s}{\partial t} = \nabla^2 T_s + H\gamma\left(T_f - T_s\right), \tag{1b}$$

$$\frac{\partial T_f}{\partial t} + \mathbf{v}\cdot\nabla T_f = \nabla^2 T_f - H\left(T_f - T_s\right). \tag{1c}$$

While the dimensionless boundary conditions used in Eqs (3) are summed up in Fig. 1 as:

$$z = 0 : \frac{\partial T_f}{\partial z} = B_f\left(T_f - 1\right), \frac{\partial T_s}{\partial z} = \gamma B_f(T_s - 1), w = 0, \tag{2a}$$

$$z = 1 : \gamma\frac{\partial T_f}{\partial z} + \frac{\partial T_s}{\partial z} + 1 + \gamma = 0, T_s = T_f, w = 0. \tag{2b}$$

The notation of the vector **v** indicates the velocity field, T indicates the temperature [K] and the subscripts "s" and "f" indicate a saturating fluid phase and a solid matrix, respectively. In contrast, the dimensionless inter-heat transfer coefficient, thermal conductivity ratio, Biot number, and modified Rayleigh number in a porous medium are briefly the parameters noted as H, γ, B_f and Ra.

Eqs (1) and (2) are a virtue of scaling quantities alongside the curl operator applied to Darcy's law. The proposed scaling quantities are [19, 12]:

$$x^* \to xl, t^* \to t\frac{l^2}{\alpha_f}, \mathbf{v}^* \to (\mathrm{u}, \mathrm{v}, \mathrm{w})\frac{\varphi\ \alpha_f}{l}, T^*_{s,f}\ \to T_w + \Delta T\ T_{s,f}, \lambda_f = \alpha_f(\rho C)_f, \lambda_s = \alpha_s(\rho C)_s,$$

$$\Delta T = \frac{q_w\ l}{\lambda_m}, \lambda_m = (1-\varphi)\lambda_s + \varphi\ \lambda_f, a_m = \frac{\lambda_m}{(\rho C)_f}, \gamma = \frac{\varphi\lambda_f}{(1-\varphi)\lambda_s}, \chi = \frac{\alpha_f}{\alpha_s},$$

$$H = \frac{hl^2}{\varphi\lambda_f}, R\alpha = \frac{(1+\gamma)\beta g\Delta TKl}{\gamma\alpha_m\nu_f}, B_f = \frac{h_{w,f}l}{\lambda_f} \tag{3}$$

The superscript of the star notation refers to dimensional variables. α is the thermal diffusivity [$m^2\ s^{-1}$], T_w is the temperature of the lower wall [K], ρ is the density [$kg\ m^{-3}$], h is the inter-phase volumetric heat transfer coefficient [$W\ (m^3\ K^{-1})$], e_z unit vector in the z-direction, C is the heat capacity per unit of mass [$J\ (kg\ K^{-1})$], q_w is the heat flux at the upper wall [$W\ m^{-2}$], ν_f is the kinematic viscosity [$m^2\ s^{-1}$], g is the modulus of the gravitational acceleration [$m\ s^{-2}$], β is thermal expansion coefficient [K^{-1}], t is the time [s] and 1 is the thickness of the layer [m]. The subscript "w" means the wall while the symbol "m" denotes the effective. λ is the thermal conductivity [$W\ (m\ K^{-1})$], $h_{w,f}$ is the superficial heat transfer coefficient of the fluid phase [$W\ (m^2\ K^{-1})$], K is the permeability of the medium [m^2].

3. BASIC STATE

The basic profile assumed for Eqs (1) and (2) is a steady state with zero velocity that fluid exists in a solid skeleton. Consequently, the basic profile is:

$$\mathbf{v}_b = 0 \tag{4}$$

$$T_{s,b} = \frac{-\left(2B_f(1-z)\gamma\sqrt{\Lambda} + (1+\gamma)^{\frac{3}{2}}\sqrt{\frac{\Lambda}{1+\gamma}}\right)\cosh\sqrt{\Lambda} - B_f(1+\gamma\left(\gamma + B_f(z-1)(1+\gamma)\right)\sinh(z-1)\sqrt{\Lambda}}{B_f(2\gamma\sqrt{\Lambda}\cosh\sqrt{\Lambda} + B_f\gamma(1+\gamma)\sinh\sqrt{\Lambda}} \tag{5}$$

$$T_{f,b} = \frac{-\left(2B_f(1-z)\gamma\sqrt{\Lambda} + (1+\gamma)^{\frac{3}{2}}\sqrt{\frac{\Lambda}{1+\gamma}}\right)\cosh\sqrt{\Lambda} + B_f(1+\gamma\left(\gamma + B_f(z-1)(1+\gamma)\right)\sinh(z-1)\sqrt{\Lambda}}{B_f(2\gamma\sqrt{\Lambda}\cosh\sqrt{\Lambda} + B_f\gamma(1+\gamma)\sinh\sqrt{\Lambda}} \tag{6}$$

Where: $\Lambda = H(1+\gamma)$

We have used the subscript "b" as a symbol of the basic flow.

The first derivative of $T_{f,b}$ that will be adopted in the governing equations is

$$T'_{f,b} = -1 + \frac{(-1+\gamma)\sqrt{\Lambda}\cosh\left[(-1+y)\sqrt{\Lambda}\right]}{2\gamma\sqrt{\Lambda}\cosh[\sqrt{\Lambda}] + Bf\gamma(1+\gamma)\sinh[\sqrt{\Lambda}]} \tag{7}$$

3.1. Basic state for local thermal equilibrium cases

The cases where the temperature of solid structure matches the fluid phase can emerge through two different limits:

a) The limiting case of $H \to \infty$ with $\gamma \approx O(1)$ that refers to the basic temperature profile of both phases as

$$T_{sb} = T_{fb} = -\frac{1+\gamma+2\gamma B_f(1-z)}{2\gamma B_f}. \tag{8}$$

b) The case of $\gamma \to \infty$ with $H \approx O(1)$ whose basic temperature profile is,

$$T_{sb} = T_{fb} = 1 - z - \frac{1}{B_f}. \tag{9}$$

3.2. Basic state for local thermal non-equilibrium cases

There are two limits in which we can have two autonomous temperature profiles: $H \to 0$ with $\gamma \approx O(1)$ or $\gamma \to 0$ with $H \approx O(1)$.The basic temperature profile for both phases in the former limit is

$$T_{fb} = -\frac{1+\gamma+{B_f}^2(-1+z)\gamma(1+\gamma) + B_f(z+(-1+z)\gamma+\gamma^2)}{B_f\gamma\left(2+B_f+B_f\gamma\right)}, \tag{10a}$$

$$T_{sb} = -\frac{1+B_f+\gamma+B_f\left(1+B_f\right)(-1+z)\gamma + B_f\left(B_f(-1+z)+z\right)\gamma^2}{B_f\gamma\left(2+B_f+B_f\gamma\right)}. \tag{10b}$$

While in the latter one it is

$$T_{fb} = \frac{e^{-\sqrt{H}z}\left(e^{2\sqrt{H}} - e^{2\sqrt{H}z} + e^{\sqrt{H}z}\left(1+B_f(-1+z)\right) + e^{\sqrt{H}(2+z)}\left(-1+B_f-B_fz\right)\right)\left(-1+\coth[\sqrt{H}]\right)}{2B_f}, \tag{11a}$$

$$T_{sb} = 1 - \frac{1}{B_f} - z. \tag{11b}$$

The basic temperature profile for all cases is expressed following the condition of $\varphi = 1/2$. Therefore, the Biot number of the solid phase can be replaced by the fluid one through the relation of $B_s = \gamma B_f$. For instance, some authors [20] have adopted this relation as a condition in the numerical method to look for the critical value of $B_s \neq B_f$ without mentioning anything related to the basic temperature profile for $\varphi = 1/2$. This in turn exhibits a discrepancy between our basic temperature profiles and the one cited in [20], knowing that they have employed the same thermal boundary conditions as we did.

4. STABILITY ANALYSIS

The basic solution is investigated by using the perturbation process which defines the main flow of each variable as a sum between the basic state and the distributed flow. More precisely,

$$T_{f,s} = T_{fs,b} + \varepsilon\tilde{T}_{fs}, \boldsymbol{v} = \boldsymbol{v}_b + \varepsilon\tilde{\boldsymbol{v}} \tag{12}$$

According to linearization method, all the second orders of ε are cancelled in Eqs (1) and (2). Thus, we can obtain:

$$\nabla\times\tilde{\boldsymbol{v}} = Ra\nabla\times\left(\tilde{T}_f\boldsymbol{e_z}\right), \tag{13a}$$

$$\chi\frac{\partial\tilde{T}_s}{\partial t} = \nabla^2\tilde{T}_s + H\gamma\left(\tilde{T}_f - \tilde{T}_s\right), \tag{13b}$$

$$\frac{\partial \tilde{T}_f}{\partial t} + \tilde{w}T'_{f,b} = \nabla^2 \tilde{T}_f + H\left(\tilde{T}_s - \tilde{T}_f\right), \tag{13c}$$

$$z = 0 : \frac{\partial \tilde{T}_f}{\partial z} = B_f\left(\tilde{T}_f - 1\right), \frac{\partial \tilde{T}_s}{\partial z} = \gamma B_f\left(\tilde{T}_s - 1\right), \tilde{w} = 0 \tag{13d}$$

$$z = 1 : \gamma\frac{\partial \tilde{T}_f}{\partial z} + \frac{\partial \tilde{T}_s}{\partial z} + 1 + \gamma = 0, \tilde{T}_s = \tilde{T}_f, \tilde{w} = 0. \tag{13e}$$

The governing equations are invariable with respect to rotation around the z-axis. We consider velocity perturbations in the two-dimensional plane (x, z), in the form of perturbed stream function $\tilde{\psi}(x, z)$:

$$\tilde{u} = \frac{\partial \tilde{\psi}}{\partial z}, \tilde{w} = -\frac{\partial \tilde{\psi}}{\partial x} \tag{14}$$

The normal modes method allows us to tackle the perturbed equations by expressing the small secondary flow as

$$\left\{\tilde{\psi}(x, z, t), \tilde{T}_{fs}(x, z, t)\right\} = \left\{i\,\Psi(z), \theta_{fs}(z)\right\}e^{i(kx-\omega t)} \tag{15}$$

Hence the symbols of $\Psi(z)$ and $\theta(z)$ are used to describe the perturbation amplitude functions. The wave number is defined by the symbol k while the growth rate and the angular frequency are noted with $\omega_i = Im\{\omega\}$ and $\omega_r = \mathrm{Re}\{\omega\}$ respectively. The complex parameter ω is defined as the sum of the imaginary and real parts of ω.

The linear stability analysis is focused only on those modes whose growth rate is neither growing nor decaying with time. This feature implies the condition of $\omega_i = 0$. Therefore, substituting Eqs (14) and (15) into Eqs (13) with $\omega_i = 0$ yields that,

$$\Psi'' - k^2\Psi + k\,Ra\,\theta_f = 0 \tag{16a}$$

$$\theta''_s - k^2\theta_s + \gamma\,H\,\left(\theta_f - \theta_s\right) + i\,\omega_r\chi\theta_s = 0 \tag{16b}$$

$$\theta''_f - k^2\theta_f + H\left(\theta_s - \theta_f\right) + kT'_f\Psi + i\omega_r\theta_f = 0 \tag{16c}$$

$$z = 0 : \theta'_f = B_f\theta_f, \theta'_s = \gamma B_f\theta_s, \Psi = 0 \tag{16d}$$

$$z = 1 : \gamma\theta'_f + \theta'_s = 0, \theta_s = \theta_f, \Psi = 0 \tag{16e}$$

The two primes in Eqs (16) mean a second derivative with respect to z.

5. THE PRINCIPLE OF EXCHANGE OF INSTABILITIES

As the principal of exchange of instabilities cannot be proven analytically owing to the variable coefficients that arise in the expression of $T'_{f,b}(z)$ in Eq. (7), we will be obligated to verify its validity through the numerical solution presented in section (6) by using the eigenvalue problem written in Eqs (16). To satisfy this principle we must obtain numerically the value of $\omega_r = \mathrm{Re}\{\omega\} = 0$. In other words, the fluid layer has to be without oscillatory instability behaviour.

According to the outcomes of Table 1 the condition of $\omega_r = \mathrm{Re}\{\omega\} = 0$ is fulfilled as all the values are nearer to zero, thus, the principle exchange of instabilities is held. Consequently, we can neglect ω_r from the eigenvalue problem Eqs (16) and write that

$$\Psi'' - k^2\Psi + k\,Ra\,\theta_f = 0 \tag{17a}$$

$$\theta''_s - k^2\theta_s + \gamma\,H\,\left(\theta_f - \theta_s\right) = 0 \tag{17b}$$

$$\theta''_f - k^2\theta_f + H\left(\theta_s - \theta_f\right) + kT'_f\Psi = 0 \tag{17c}$$

$$z = 0 : \theta'_f = B_f\theta_f, \theta'_s = \gamma B_f\theta_s, \Psi = 0 \tag{17d}$$

$$z = 1 : \gamma\theta'_f + \theta'_s = 0, \theta_s = \theta_f, \Psi = 0 \tag{17e}$$

6. NUMERICAL SOLUTIONS

The numerical solutions proposed for the eigenvalue problem Eqs (17) are based on the two combined procedures carried out between the Runge-Kutta solver and the finding-root algorithm of the shooting method. To apply both of them, we need to switch Eqs (17) into an initial value problem by providing other boundary conditions to Eq. (17d),

$$\Psi(0) = 1, \theta_f = s_1, \theta_s = s_2 \tag{18}$$

We take into consideration the normalisation condition of $\Psi(0) = 1$. The two unknown's parameters s_1 and s_2 are

Table 1. The real values of ω_r calculated by the numerical method of the Runge-Kutta solver and shooting method

$H = 10^{-2}$ and $B_f = 10$				$H = 10^{2}$ and $B_f = 10$			
$\gamma = 10^{-1}$		$\gamma = 10$		$\gamma = 10^{-1}$		$\gamma = 10$	
k	ω_r	k	ω_r	k	ω_r	k	ω_r
1	2.260839×10^{-21}	1	1.049347×10^{-18}	1	1.657385×10^{-18}	1	9.989764×10^{-6}
2	9.074241×10^{-22}	2	4.309620×10^{-18}	2	8.040071×10^{-16}	2	9.948204×10^{-6}
3	3.932491×10^{-21}	3	9.037235×10^{-18}	3	2.885237×10^{-15}	3	9.582209×10^{-6}
4	7.540579×10^{-21}	4	1.569522×10^{-17}	4	3.826143×10^{-14}	4	9.666727×10^{-6}
5	1.298220×10^{-20}	5	2.674431×10^{-17}	5	7.646567×10^{-15}	5	9.269420×10^{-6}
6	2.027311×10^{-20}	6	4.297010×10^{-17}	6	4.574078×10^{-15}	6	9.209937×10^{-6}

defined as values for $\theta_s(0)$ and $\theta_f(0)$, in the meantime they are assigned as one of those input parameters fixed in the shooting method. This latter is also implemented via the function Find Root of the Mathematica10 software. In general, the process employed here allows us to develop accurate values for s_1, s_2 and Ra. The resulting function of $Ra(k)$ is employed to draw the marginal stability curves for every input parameter (H, γ, B_f).

Table 2 shows a comparison of the critical values noted for work [20] in the case where Robin and Neumann thermal boundary conditions are used with the presence of the free surface, and the critical values calculated for our problem with the same thermal conditions but with rigid impermeable walls. If we look at the modified Rayleigh number defined in this paper Eq. (3) is the same as the one employed in [12] and not the one used by [20]. The incongruence in the definition will make the comparison of the results a little bit unclear or hardly seen. To overcome this discrepancy, we calculate the critical values for both R_c and Ra_c by considering the same conditions γ, B_f and H, mentioned in [20]. From Table 1 we can remark that the values of R_c and Ra_c in our problem differ from one another. This is somehow contrasted with what arises in the Brinkman problem whose R_c and Ra_c are nearly equal (see [11]). As a consequence, the parameter γ has a more vital impact on Darcy's configuration than Brinkman one. On the other hand, the results in [20] point out that as much as γ decreases, the R_c goes closer to zero, in other words, the basic flow becomes alone unstable when $\gamma \to 0$. Overall, this limiting case makes the effect of other parameters on the instability behaviour unseen, and this why we have taken by preference the definition of Ra_c rather than R_c. The difference between the critical values in both studied cases does not depend only on the definition of R_c but also on the hydrodynamic boundary conditions employed by each problem. As is well known the instability in a porous layer emerges at low critical values in the case of an open boundary than an impermeable wall. This in general upholds the finding results in Table 2.

7. RESULTS AND DISCUSSION

The frames in Figs 2–5 present the trends of Ra_c and k_c versus B_f with various values of γ while the marginal curves

Table 2. Comparison of Celli et al. [20] results with the study problem

$B_f = 1$ and $H = 0.1$						
The work of Celli et al. [20]			The studied problem			
γ	k_c	R_c	γ	k_c	R_c	$Ra_c = \frac{1+\gamma}{\gamma}R_c$
1	1.40561	5.01644	1	2.06170	12.22724	24.45449
0.5	1.51745	3.68189	0.5	2.23459	8.82849	26.48548
0.25	1.62350	2.38060	0.25	2.38631	5.62602	28.13013

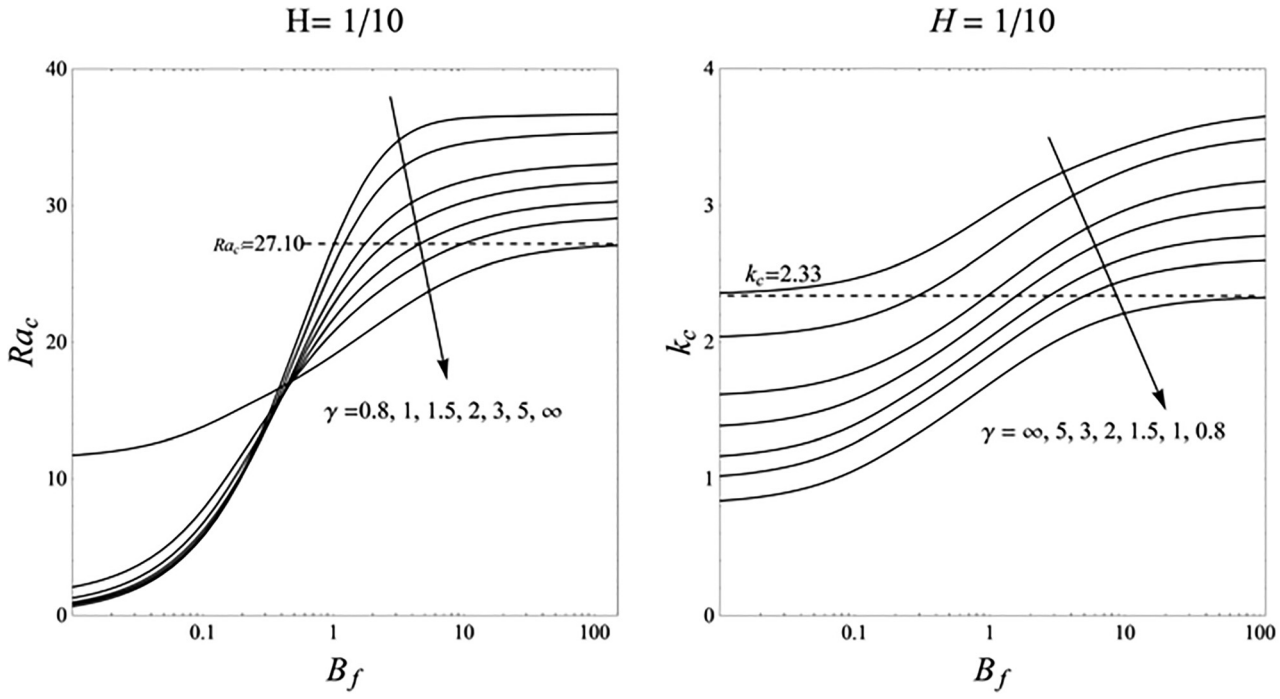

Fig. 2. The plots of Ra_c and k_c versus B_f for $H = 1/10$

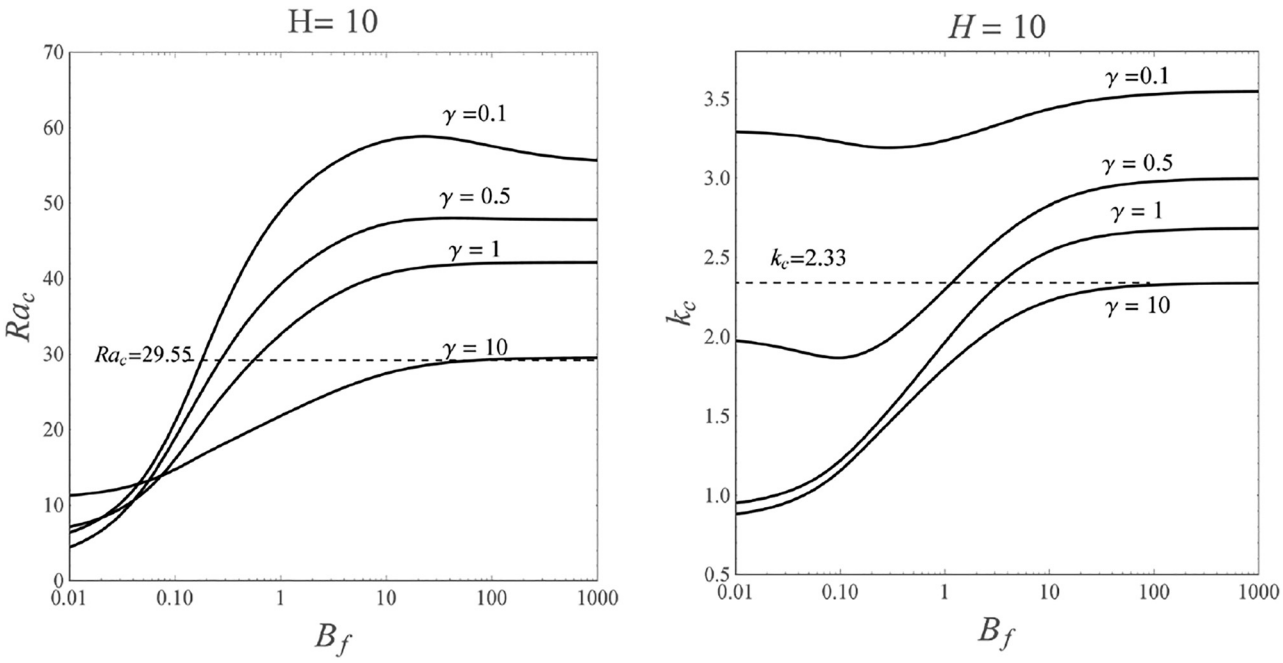

Fig. 3. The trends of Ra_c and k_c versus B_f for $H = 10$

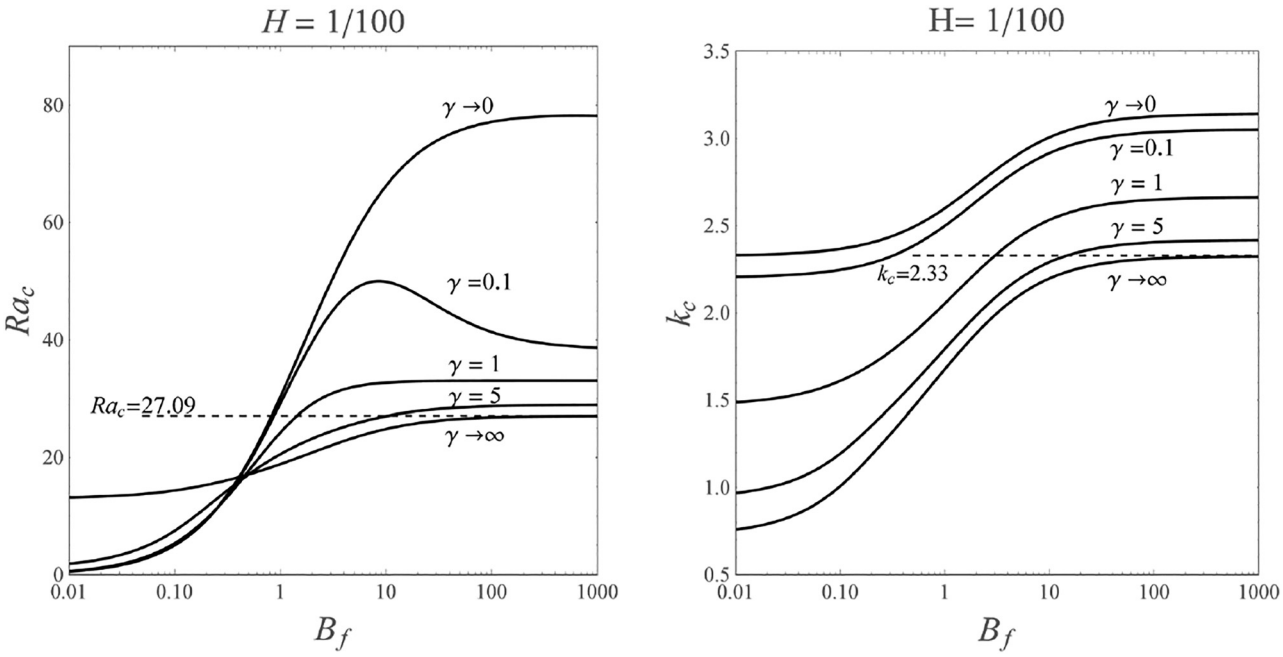

Fig. 4. The trends of Ra_c and k_c versus B_f for $H = 1/100$

drawn for γ and H with fixed B_f are displayed in Fig. 6. The dashed line describes the critical value of Ra_c and k_c obtained for cases close to the LTE model. We recall that stability always exists in the region situated below the concave shape of the neutral curves, while instability emerges in the area above the concave curves. In Fig. 6 the right frame reveals that decreasing the values of γ tend the marginal stability curves to move continuously upward, therefore prescribing a more stable state. In addition, the results that emerge from Figs 2–5 ensure a non-monotonic increase of the critical values with respect to γ. Furthermore, the effect of $\gamma \to 0$ does not seem to neglect the influence of H as $Ra_c = \infty$ with $H \to \infty$. This feature enables the basic state to behave as adiabatic conditions. Regardless of the effect of H, the limit of $\gamma \to \infty$ leads the values of Ra_c and k_c to be nearly as $Ra_c = 27.10$, $k_c = 2.33$ apart from the ones in Fig. 3 and in Fig. 5 whose critical values are different, this refers to the definition of Ra_c. Therefore, a higher value of γ can be regarded as

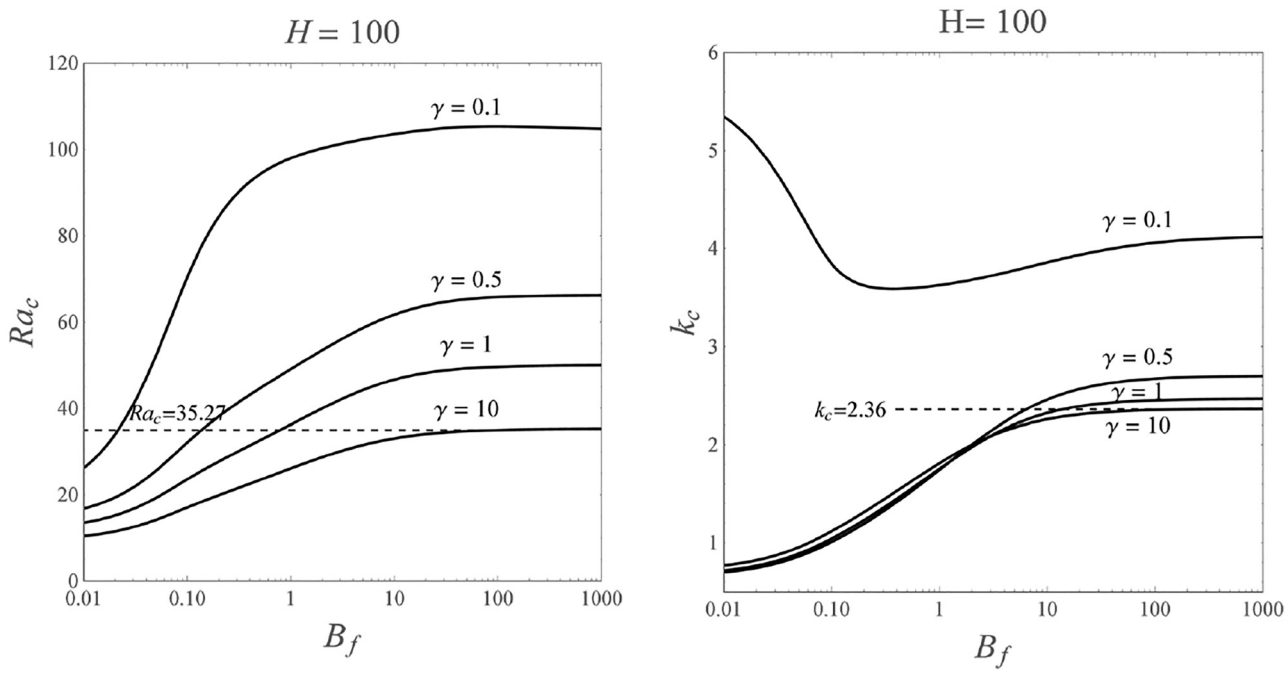

Fig. 5. The plots of Ra_c and k_c versus B_f for $H = 100$

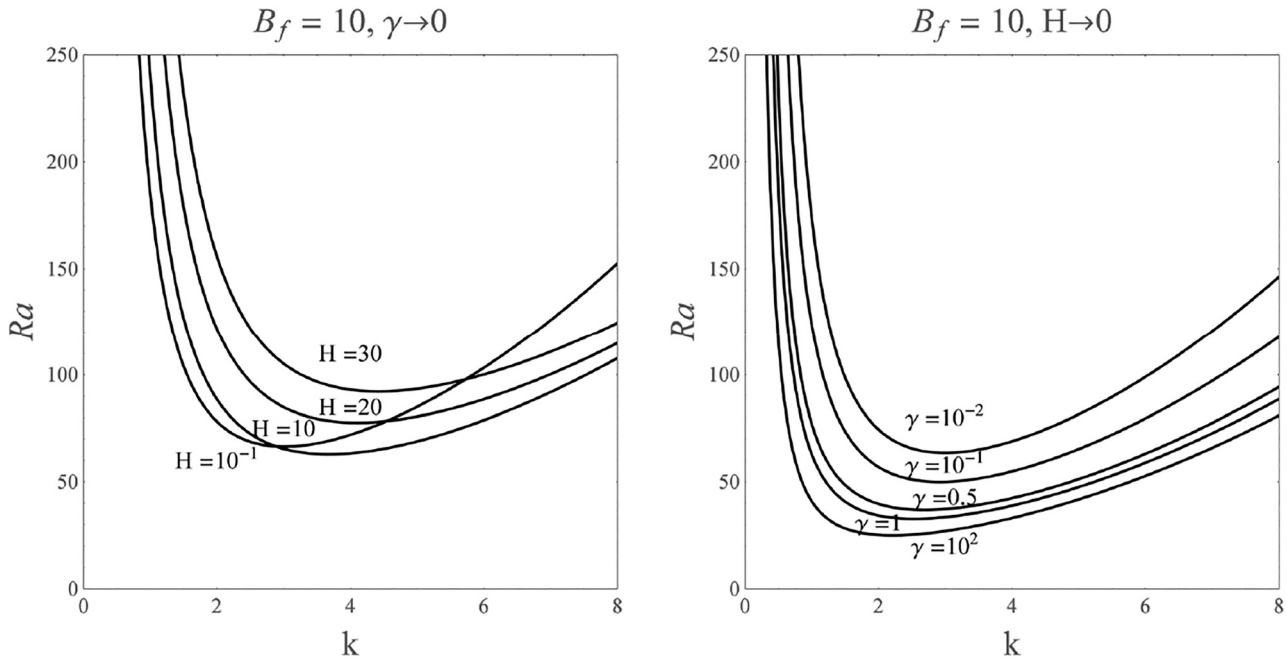

Fig. 6. Marginal stability curves relative to $H \to 0$ (right frame) and $\gamma \to 0$ (left frame)

one of the destabilizing factors in this case. Otherwise, the growth of H can bridge the gap between LTNE and LTE when γ has a finite value and $B_f \to \infty$. In other words, the parameters of H, B_f and γ can have stabilising or destabilising effect as they are based on the thermal conductivity of the solid and fluid phase besides the inter-phase volumetric heat transfer coefficient h.

8. CONCLUSION

The studied configuration of the modified Darcy-Benard problem is an approach to the design of metal foams saturated with Newtonian fluid. The solid matrix of the metal foams has thermal conductivity infinitely higher than its counterpart fluid phase, which means the presence of the

LTNE model. This design is used as a heat exchanger to enhance the transfer of heat from the cooling Newtonian fluid to the solid body, as a result it can be a good alternative to the finned surfaces. According to the numerical results, the stability effects are much more dominant in $\gamma \to 0$ than in $\gamma \to \infty$ when no heat is transferred between the two phases. Besides, the curves *Ra* relative to $H \to 0$ exhibit more sensitivity via the value of γ when $B_f \to \infty$. Broadly speaking, the behaviour of γ, H and B_f can hasten the performance of heat exchange in metal foams between the porous layer and a saturating fluid.

ACKNOWLEDGEMENT

This research was not funded by any grant.

REFERENCES

[1] C. W. Horton and F. T. Rogers, "Convection currents in a porous medium," *J. Appl. Phys.*, vol. 16, p. 367, 1945. https://doi.org/10.1063/1.1707601.

[2] B. Wen, A. Daria, L. Zhang, and A. Hesse Marc, "Carbon dioxide dissolution in a closed porous medium at low pressure," *J. Fluid Mech.*, vol. 854, no. 10, pp. 56–87, 2018. https://doi.org/10.1017/jfm.2018.622.

[3] D. A. Nield and T. Simmons Craig, "A brief introduction to convection in porous media," *Transport Porous Media*, vol. 130, no. 10, pp. 237–50, 2018. https://doi.org/10.1007/s11242-018-1163-6.

[4] R. Dubey and P. V. S .N. Murthy, "The onset of double-diffusive convection in a Brinkman porous layer with convective thermal boundary conditions," *AIP Adv.*, vol. 9, 2019, Paper no. 045322. https://doi.org/10.1063/1.5087037.

[5] A. Bouachir, M. Mamon, R. Rebhi, and S. Benissaadi, "Linear and nonlinear stability analyses of double-diffusive convection in a vertical brinkman porous enclosure under soret and dufour effects," *Fluids*, vol. 6, no. 8, pp. 292–302, 2021. https://doi.org/10.3390/fluids6080292.

[6] A. D. Nield and A. Bejan, *Chapter 6 – Convection in Porous Media: Internal Natural Convection: Heating from below*, 4th ed. New York, Springer-Verlag, 2013, pp. 221–329, https://doi.org/10.1007/978-1-4614-5541-7_6.

[7] C. W. Horton and F. T. Rogers, "Convection currents in a porous medium," *J. Appl. Phys.*, vol. 16, no. 1, pp. 367–77, 1945. https://doi.org/10.1063/1.1707601.

[8] M. Parhizi, M. Torabi, and A. Jain, "Local thermal non-equilibrium (LTE) model for developed flow in porous media with spatially-varying biot number," *Int. J. Heat Mass Tran.*, vol. 164, pp. 1–9, 2021. https://doi.org/10.1016/j.ijheatmasstransfer.2020.120538.

[9] V. Kambiz and Y. Kun, "A note on local thermal non-equilibrium in porous media and heat flux bifurcation phenomenon in porous media," *Transport Porous Media*, vol. 96: 169–72, 2013. https://doi.org/10.1016/j.ijheatmasstransfer.2020.120538.

[10] F.-K. Arman, N. Meysam, and M. Yasser, "Pulsating Flow in a Channel Filled with a Porous Medium under local thermal non-equilibrium condition: an exact solution," *J. Therm. Anal. Calorim.*, vol. 145, no. 7, pp. 2753–75, 2020. https://doi.org/10.1007/s10973-020-09843-0.

[11] A Postelnicu and D. A. S. Rees, "The onset of Darcy-Brinkman convection in a porous layer using a thermal nonequlibrium model - Part I: stress-free boundaries," *Int. J. Energy Res.*, vol. 27, no. 10, pp. 961–73, 2003. https://doi.org/10.1002/er.928.

[12] N. Banu and D. A. S. Rees, "Onset of Darcy-Benard convection using a thermal Nonequilibrium model," *Int. J. Heat Mass Tran.*, vol. 45, no. 11: 2221–8, 2002. https://doi.org/10.1016/S0017-9310(01)00331-3.

[13] A Barletta and D. A. S Rees, "Local thermal non-equilibrium effects in the Darcy-Benard instability with isoflux boundary conditions," *Int. J. Heat Mass Tran.*, vol. 55, pp. 384–94, 2012. https://doi.org/10.1016/j.ijheatmasstransfer.2011.09.031.

[14] A. Barletta, M. Celli, and D. A. S Rees, "Buoyant flow and instability in a vertical cylindrical porous slab with permeable Boundaries," *Int. J. Heat Mass Tran.*, vol. 157, pp. 210–320, 2020. https://doi.org/10.1016/j.ijheatmasstransfer.2020.119956.

[15] A. Barletta and D. A. S Rees, "On the onset of convection in a highly permeable vertical porous layer with open boundaries," *AIP Phys. Fluids*, vol. 31, 2019, Paper no. 074106. https://doi.org/10.1063/1.5110484.

[16] A. Barletta and M. Celli, "The Horton-Rogers-Lapwood problem for an inclined porous layer with permeable boundaries," *Roy. Soc. Publish. Proc. A*, vol. 474, 2018. https://doi.org/10.1098/rspa.2018.0021.

[17] F. Al-Sumaily Gazy, A. Al Ezzi, A. Dhahad Hayder, M. C. Thompson, and T. Yusaf, "Legitimacy of the local thermal equilibrium hypothesis in porous media: a comprehensive Review," *J. Energy*, vol. 14, no. 23, pp. 2–47, 2021. https://doi.org/10.3390/en14238114.

[18] H. Lagziri and M. Bezzazi, "Robin boundary effects in the Darcy-Rayleigh problem with local thermal non equilibrium model," *Transport Porous Media*, vol. 129, no. 1, pp. 701–20, 2019. https://doi.org/10.1007/s11242-019-01301-2.

[19] A. Barletta, M. Celli, and H. Lagziri, "Instability of a horizontal porous layer with local thermal non-equilibrium: effects of free surface and convective boundary conditions," *Int. J. Heat Mass Transfer*, vol. 89, no. 1, pp. 75–89, 2015. https://doi.org/10.1016/j.ijheatmasstransfer.2015.05.026.

[20] M. Celli, H. Lagziri, and M. Bezzazi, "Local thermal non-equilibrium effects in the Horton-Rogers-Lapwood problem with a free surface," *Int. J. Therm. Sci.*, vol. 116, no. 1, 254–64, 2017. https://doi.org/10.1016/j.ijthermalsci.2017.03.001.